

A multi-methodological study of kurnakovite: a potential B-rich aggregate

G. Diego Gatta, Alessandro Guastoni, Paolo Lotti, Giorgio Guastella,
Oscar Fabelo and Maria Teresa Fernandez-Diaz

Running title: Crystal chemistry of kurnakovite

Abstract, Keywords

Introduction

Sample description and occurrence

Experimental methods

- **Titrimetric determination of boron**
- **EDTA titrimetric determination of magnesium**
- **Determination of fluorine content**
- **Determination of H₂O content by heating**
- **Determination of minor elements by inductively coupled plasma atomic emission spectroscopy (ICP-AES)**
- **Determination of REE concentration by ICP-AES**
- **Single-crystal neutron diffraction**

Discussion and Implications

Acknowledgements

References

Figures/Tables

Corresponding author: G. Diego GATTA

Dipartimento di Scienze della Terra, Università degli Studi di Milano

Via Botticelli 23, I-20133 Milano, Italy

Tel. +39 02 503 15607, Fax +39 02 503 15597, E-Mail: diego.gatta@unimi.it

Manuscript submitted to American Mineralogist

A multi-methodological study of kurnakovite: a potential B-rich aggregate

G. Diego Gatta¹, Alessandro Guastoni², Paolo Lotti¹, Giorgio Guastella³,
Oscar Fabelo⁴ and Maria Teresa Fernandez-Diaz⁴

¹Dipartimento di Scienze della Terra, Università degli Studi di Milano,
Via Botticelli 23, I-20133 Milano, Italy

²Dipartimento di Geoscienze, Università degli Studi di Padova,
Via G. Gradenigo 6, I-35131, Padova, Italy

³Agenzia delle Dogane e dei Monopoli, Direzione Regionale per la Lombardia,
Laboratorio e Servizi Chimici, Via Marco Bruto 14, I-20138 Milan, Italy

⁴Institut Laue-Langevin, 71 Avenue des Martyrs, F-38000 Grenoble, France

Abstract

The crystal structure and crystal chemistry of kurnakovite from Kramer Deposit (Kern County, California), ideally $\text{MgB}_3\text{O}_3(\text{OH})_5 \cdot 5\text{H}_2\text{O}$, was investigated by single-crystal neutron diffraction (data collected at 293 and 20 K) and by a series of analytical techniques aimed to determine its chemical composition. The concentration of more than 50 elements was measured. The empirical formula of the sample used in this study is: $\text{Mg}_{0.99}(\text{Si}_{0.01}\text{B}_{3.00})\Sigma_{3.01}\text{O}_{3.00}(\text{OH})_5 \cdot 4.98\text{H}_2\text{O}$. The fraction of rare earth elements (REE) and other minor elements is, overall, insignificant. Even the fluorine content, as potential OH-group substituent, is insignificant (*i.e.*, ~ 0.008 wt%). The neutron structure model obtained in this study, based on intensity data collected at 293 and 20 K, shows that the structure of kurnakovite contains: $[\text{BO}_2(\text{OH})]$ -groups in planar-triangular coordination (with the B-ions in sp^2 electronic configuration), $[\text{BO}_2(\text{OH})_2]$ -groups in tetrahedral coordination (with the B-ions in sp^3 electronic configuration), and $\text{Mg}(\text{OH})_2(\text{H}_2\text{O})_4$ -octahedra, connected in (neutral) $\text{Mg}(\text{H}_2\text{O})_4\text{B}_3\text{O}_3(\text{OH})_5$ units forming infinite chains running along [001]. Chains are mutually connected to give the tri-dimensional structure only *via* H-bonding, and extra-chains “zeolitic” H_2O molecules are also involved as “bridging molecules”. All the oxygen sites in the structure of kurnakovite are involved in H-bonding, as *donors* or as *acceptors*.

The principal implications of these results are: 1) kurnakovite does not act as geochemical trap of industrially relevant elements (*e.g.*, Li, Be or REE), 2) the almost ideal composition makes kurnakovite a potentially good B-rich aggregate in concretes (used *e.g.* for the production of radiation-shielding materials for the elevated ability of ^{10}B to absorb thermal neutrons) avoiding the

71 risk to release undesirable elements, for example sodium, which could promote deleterious reactions
72 for the durability of cements.

73

74 **Keywords:** kurnakovite, borates, single-crystal neutron diffraction, crystal chemistry, hydrogen
75 bonding, B-rich aggregate.

76

77 **Introduction**

78 Kurnakovite, with ideal chemical formula $\text{MgB}_3\text{O}_3(\text{OH})_5 \cdot 5\text{H}_2\text{O}$, is a complex hydrous borate
79 mineral found as a common constituent of borate deposits, along with borax (ideally
80 $\text{Na}_2(\text{B}_4\text{O}_5)(\text{OH})_4 \cdot 8\text{H}_2\text{O}$) and ulexite (ideally $\text{NaCa}[\text{B}_5\text{O}_6(\text{OH})_6] \cdot 5\text{H}_2\text{O}$). Natural borates represent the
81 most important source of boron, an important geochemical marker for petrogenetic processes (especially
82 in pegmatitic and granitic systems) and a strategic element for technological materials (*e.g.*, to lower
83 melting temperatures and melt viscosities in silicate glass systems), but are also being used for the
84 production of radiation-shielding materials for the elevated ability of ^{10}B to absorb thermal neutrons.
85 More specifically, the most important utilizations are referred to radiation emitted by nuclear reactors
86 for energy production, scientific research or medical applications, which promoted the development of
87 suitable materials able to shield from harmful radiations. Approximately 20% of natural boron is ^{10}B ,
88 which shows a high capacity to absorb thermal neutrons due to its high cross section for the $^{10}\text{B}(\text{n},\alpha)^7\text{Li}$
89 reaction (~ 3840 barns; Carter et al. 1953, Palmer and Swihart 1996, Rauch and Waschkowski 2002).
90 Borax and ulexite have been object of investigations in order to produce B-rich aggregates in concretes.
91 However, these two minerals have proved to induce a drastic effect on setting and hardening, coupled
92 with a drastic lowering of strength development and durability of concretes (*e.g.*, Glinicki et al. 2018).
93 In addition, these minerals dissolve into the paste releasing sodium, which could potentially promotes
94 deleterious reactions for the durability of Portland cements. On the other hand, the use of most stable
95 compounds, like *e.g.* the synthetic B_4C or B-mullites, is not environmentally and economically
96 sustainable (Okumo et al. 2009, Gatta et al. 2013, Di Julio et al. 2017). In the framework of a long term
97 project to select new potential substituents of borax and ulexite as B-bearing aggregates, we have recently
98 investigated the crystal chemistry, the stability at high and low temperature (Lotti et al. 2018, 2019) and
99 at high pressure (Lotti et al. 2017) of colemanite (ideally $\text{CaB}_3\text{O}_4(\text{OH})_3 \cdot \text{H}_2\text{O}$), using a multi-
100 methodological approach. We now extend our investigation to kurnakovite, a Na-free borate with B_2O_3
101 $\approx 37\text{wt}\%$, starting with a careful crystal-chemical investigation, which will be followed by experiments
102 on its chemical and *P-T* stability.

103 Only a few studies were devoted to this mineral and to its dimorph inderite. After preliminary (and
104 incomplete) data about the crystallographic features of kurnakovite (Petch et al. 1962), its first structure
105 model was reported by Razmanova et al. (1969), and later refined by Corazza (1974) on the basis of
106 single-crystal X-ray Weissenberg data, in the space group $P-1$ with $a \approx 8.35 \text{ \AA}$, $b \approx 10.61 \text{ \AA}$, $c \approx 6.44 \text{ \AA}$,
107 $\alpha \approx 98.8^\circ$, $\beta \approx 109.0^\circ$, $\gamma \approx 105.6^\circ$ ($V \approx 501.2 \text{ \AA}^3$). No more recent structural refinements are reported in
108 the literature. ^{11}B and ^{25}Mg NMR data and DFT calculations of the crystal structure of inderite and
109 kurnakovite were recently reported by Zhou et al. (2012). Following the model of Corazza (1974), the
110 structure of kurnakovite contains: $[\text{BO}_2(\text{OH})]$ -groups in triangular coordination, $[\text{BO}_2(\text{OH})_2]$ -groups in
111 tetrahedral coordination, and $\text{Mg}(\text{OH})_2(\text{H}_2\text{O})_4$ octahedra, connected in (neutral) $\text{Mg}(\text{H}_2\text{O})_4\text{B}_3\text{O}_3(\text{OH})_5$
112 units forming chains running along the $[001]$ direction (Fig. 1). “Zeolitic” H_2O molecules populate small
113 cavities, H-bonded to the aforementioned chains. The major difference between the dimorphs
114 kurnakovite and inderite lies in the linkage of the $\text{Mg}(\text{H}_2\text{O})_4\text{B}_3\text{O}_3(\text{OH})_5$ unit: in inderite this unit consists
115 of the triborate ring and $\text{Mg}(\text{OH})_2(\text{H}_2\text{O})_4$ octahedron sharing two OH groups, whereas in kurnakovite
116 the unit is composed of alternating triborate rings and $\text{Mg}(\text{OH})_2(\text{H}_2\text{O})_4$ octahedra, sharing one oxygen
117 atom to form infinite chains (Fig. 1).

118 The X-ray refinement model of Corazza (1974) provided the position of H-sites in the structure of
119 kurnakovite, and a general description of the hydrogen bonds acting as linkage between the $[001]$ -chains.
120 No chemical analysis was performed on the investigated material by Corazza (1974), assuming the ideal
121 chemical composition of the mineral previously reported by Razmanova et al. (1969). Despite the general
122 structure model appears to be consistent (in terms of bond distances and angles), the structure refinement
123 of Corazza (1974) provides only a partial view of the H-bonding configuration, due to the limitation of
124 the X-ray diffraction at that time. In addition, some differences between the structure model of
125 Razmanova et al. (1969) and Corazza (1974) actually occur. Kurnakovite is one of the few minerals that
126 contain hydroxyl groups, cation-coordinated H_2O molecules and “zeolitic” H_2O molecules, and therefore
127 a model with an accurate location of the H-sites is necessary. In this light, and considering the expected
128 important role played by the H-bonding network on the phase stability of kurnakovite (*i.e.*, the overall
129 H_2O content is $\sim 48 \text{ wt\%}$), the aim of the present study is a reinvestigation of the crystal structure and
130 crystal chemistry of kurnakovite by single-crystal neutron diffraction at room and low temperature (20
131 K) along with a series of other analytical techniques (*i.e.*, titrimetric analysis for the determination of B
132 and Mg content, inductively coupled plasma atomic emission spectroscopy - ICP-AES - for REE and
133 other minor elements, ion selective electrode for F, high- T mass loss for H_2O content). The combination
134 of these techniques is expected to provide:

- 135 a) an unambiguous location of all the proton sites and the description of the complex H-bonding
136 network in the kurnakovite structure, along its low- T induced rearrangement;
- 137 b) the anisotropic displacement parameters of all the atomic sites, including the H-sites;
- 138 c) a more robust description of B-coordination environment (*e.g.*, aplanarity of the $\text{BO}_2(\text{OH})$ -group,
139 tetrahedral distortion of the $\text{BO}_2(\text{OH})_2$ -groups);
- 140 d) a description of the crystal chemistry of this mineral based on modern analytical protocols, with
141 a particular attention to the potential B- and Mg-substituents.

142 The experiments at low T have been performed as the vibrational regime of protons at room- T can
143 give rise to some dynamic or static disorder, which is minimised at low T . We expect that the
144 experimental findings of the present crystal-chemical investigation will be pivotal to fully understand
145 the chemical and P - T stability of this mineral, for its potential use as environmentally and economically
146 sustainable (mineral) B-bearing aggregates in Portland, Sorel or other types of cements.

147

148 **Sample description and occurrence**

149 The sample of kurnakovite used in this study belongs to the collection of the Museum of
150 Mineralogy of the University of Padova (Italy). A fragment of a large translucent crystal, measuring
151 20 centimeter as maximum length and showing a combination of well-formed euhedral pinacoids,
152 was used. The specimen was collected at the Kramer Deposit, Mohave desert, Kern County,
153 California. In 1913, this boron deposit was accidentally discovered when a well was drilled for water
154 in the Mohave desert and it penetrated the bedrock beneath the alluvium reaching the colemanite-
155 bearing stratigraphic layer (Noble 1926). The production of borax and other borates began in 1927
156 and continued until 1957, when the diggings changed to open pit quarry.

157 The geologic setting of the kurnakovite deposit is imperfectly known. The borate minerals,
158 several hundred feet underground, occur in a complex clay series, underlain by igneous rocks
159 composed by basaltic lavas, upper Miocenic in age and overlain by a stratigraphic series of
160 continental arkosic sands (Siefke 1991). The deposit has been dated as upper Miocenic on the basis
161 of mammalian fossils discovered above borates (Whistler 1984). The Kramer deposit consists of a
162 lenticular mass of borax and subordinate ulexite, colemanite, kernite and kurnakovite, measuring 1.6
163 km long, 0.8 wide and up to 100 m thick. The bed of basaltic lava underlying the borate deposits is
164 believed have been poured out and to be indirectly the source of boron, which was derived from the
165 hot springs and solfataras connected with the Tertiary volcanic activity. Tuffaceous clay beds,
166 showing ripple marks as well, occur interbedded with borax (Obert and Long 1962).

167 More than 80 minerals have been reported occurring in the Kramer deposit including a number
168 of borates as borax, colemanite, greigite, hydroboracite, inderite, inyoite, kernite, kurnakovite,
169 meyerhofferite, probertite, searlesite, tincalconite, tunellite and ulexite. No evidence of the most
170 common evaporite minerals, like halite and gypsum, were found associated to primary borax and
171 other borates beds (Schaller 1930, Morgan and Erd 1969, Puffer 1975).

172

173 **Experimental methods**

174

175 **1) Titrimetric determination of boron**

176 A mass of 80-100 mg of sample of kurnakovite was placed in a 50 ml plastic test tube, along
177 with 5 ml of water and 3 ml of hydrochloric acid 1M; the plastic test tube was then covered and
178 transferred in an ultrasound bath for 1-2 hours. The resulting clear solution was transferred in a 200-
179 300 ml beaker with water up to about 100 ml of total solution. A combined glass electrode (InLab®
180 Routine Pro – Mettler Toledo) was immersed in the solution and the pH was adjusted to 5.5-6.5 with
181 solutions of HCl 0.1-1M and NaOH 0.1-1M. 5-6 grams of mannitol were added and stirred until the
182 complete dissolution of the solid. The solution was then titrated with NaOH 0.1M up to pH 8.3-8.7.
183 The content of acid titrated was entirely due to the presence of boric acid in solution, as the sample
184 does not contain elements capable to hydrolyze the medium, or in general able to influence its acidity.
185 The measured fraction of B₂O₃ was 37.3(3) wt%.

186

187 **2) EDTA titrimetric determination of magnesium**

188 A mass of 40-80 mg of mineral sample was placed in a 50 ml plastic test tube, along with 5
189 ml of water and 1 ml of hydrochloric acid 1M; the plastic tube was covered with lid and transferred
190 in an ultrasound bath for 1-2 hours. The resulting clear solution was transferred in a 300-400 ml
191 beaker and diluted to 200 ml with water. 10 ml of buffer solution (pH 10 mixture ammonium
192 chloride/ammonia) and 3-4 drops of Eriochrome black T solution (2 g/l in ethanol) were added. The
193 solution was then titrated with standard solution of EDTA (ethylenediaminetetra-acetic acid) 0.01 M.
194 The end point was reached when the reddish purple colour of the solution was altered to blue. The
195 total volume of EDTA used was assumed to be related to the average of magnesium content of the
196 sample. The resulting fraction of MgO was 14.3(2) wt%.

197

198 **3) Determination of fluorine content**

199 20 mg of mineral sample was placed in a 50 ml plastic test tube, along with 5 ml of water and
200 3 ml of hydrochloric acid 1M; the plastic test tube was covered and transferred in an ultrasound bath
201 for 1-2 hours. 2-3 ml of Total Ionic Strength Adjustment Buffer (commercial solution TISAB III)
202 were added to the clear solution and diluted to 20 ml with water. The F content was then determined
203 using the perfectION™ Combination Fluoride Ion Selective Electrode (Mettler Toledo), adopting the
204 well-known addition method of Certified Reference Materials - CRM solution of fluorine from 0.1
205 to 5.0 mg/l. The resulting F fraction was 0.008 wt% (uncertainty not determined).

206

207 4) **Determination of H₂O content by heating**

208 500-600 mg of sample was placed in a quartz crucible with lid, and gradually heated in a
209 muffle furnace from ambient temperature up to 800°C. Assuming that the mass loss represents the
210 total amount of H₂O, the estimated fraction of H₂O of the sample was 48.2(2) wt%.

211

212 5) **Determination of minor elements by inductively coupled plasma atomic emission** 213 **spectroscopy (ICP-AES)**

214 All measurements were performed in axial view mode for REE and radial view mode for the
215 other minor elements with a Perkin Elmer Optima 7000DV ICP-AES spectrometer.

216

217 5.1) **Determination of REE concentration by ICP-AES**

218 50 mg of mineral sample was placed in a 50 ml plastic test tube, along with 5 ml of water and
219 3 ml of hydrochloric acid 1M; plastic test tube was covered and transferred in an ultrasound bath for
220 1-2 hours. The resulting clear solution was then transferred and diluted with water in a 50 ml
221 volumetric flask. A calibration protocol was performed with a blank solution and a series of solutions
222 prepared with: similar fractions of magnesium and boron as those of the sample under investigation
223 and REE concentration from 0.001 to 0.050 mg/l for each element (using CRM multi elemental
224 standard mix for ICP). Results and instrumental parameters are listed in Table 1.

225

226 5.2) **Determination of other minor elements concentration by ICP-AES**

227 For the non-REE minor elements determination, two different protocols were used:

- 228 i) 10-20 mg of mineral sample was placed in a 50 ml plastic test tube, along with 5 ml
229 of water and 3 ml of hydrochloric acid 1M; the plastic test tube was covered and
230 transferred in an ultrasound bath for 1-2 hours. The resulting clear solution was
231 transferred and diluted with water in a 25 ml volumetric flask containing 2.5 ml of

232 scandium solution 100 mg/l as internal standard. A calibration protocol was performed
233 with a blank solution and a series of 5 solutions prepared with concentration from 0.05
234 to 1.0 mg/l for each element (using CRM multi elemental standard mix for ICP).

235 ii) Decomposition by alkaline fusion of 10-20 mg of mineral sample in platinum crucible
236 with 100 mg of sodium carbonate or potassium carbonate in a muffle furnace at
237 1000°C for 5 minutes, followed by dissolution in 10 ml of water and 1 ml of sulfuric
238 acid 1M or 1 ml of hydrochloric acid 1M. The clear solution was then transferred and
239 diluted with water in a 25 ml volumetric flask containing 2.5 ml of scandium solution
240 100 mg/l as internal standard. A calibration protocol was performed with a blank
241 solution and a series of 5 solutions prepared with concentration from 0.05 to 1.0 mg/l
242 for each element (using CRM multi elemental standard mix for ICP). Results and
243 instrumental parameters are listed in Table 2.

244

245 A representative chemical analysis of kurnakovite from Kramer Deposit, and its empirical
246 formula recalculated on the basis of 13 anions, is given in Table 3.

247

248

249 **6) Single-crystal neutron diffraction**

250 A first set of single-crystal neutron diffraction data was collected at room temperature from a
251 fragment of kurnakovite (approx. 3 x 4 x 4 mm³) on the four-circle diffractometer D9 at the Institut
252 Laue-Langevin (ILL), Grenoble. The wavelength of 0.8377(1) Å, obtained from a Cu(220)
253 monochromator, and a small two-dimensional area detector were used. The measurement strategy
254 consisted of a series of ω -scans or ω -2 θ scans for low and high-Q reflections, respectively. The
255 reflections were collected varying the ω -range as a function of the instrument resolution curve. A
256 total number of 2252 reflections were collected. The integration, background and Lorentz factor
257 correction of the scans were done with the program RACER (Wilkinson et al. 1988). The lattice was
258 found to be metrically triclinic, as previously reported by Corazza (1974).

259 A further set of data from the same crystal was collected at room T on the monochromatic
260 four-circle diffractometer D19 at ILL. The wavelength used was 1.4538(1) Å, provided by a flat
261 Cu(220) monochromator (at $2\theta_M = 69.91^\circ$ take-off angle). The measurement strategy consisted of a
262 series of ω -scans with steps of 0.07° at different χ and ϕ positions, with 2123 collected reflections.
263 The data collection was performed using the Multi-Detector Acquisition Data Software (MAD) from
264 ILL. Indexing and unit-cell determination was done by using PFIND and DIRAX programs

265 (Duisenberg 1992). The integration of the raw data and refinement of the UB-matrix, including the
266 off-sets, were done using RETREAT and RAFD19 programs, respectively, along with the Lorentz
267 correction of the intensities (Wilkinson et al. 1988). The lattice was found to be metrically triclinic,
268 according to the first data set collected on D9. The absorption correction was carried out using D19abs
269 program (Matthewman et al. 1982).

270 Considering the two sets of data at room temperature (*i.e.*, 293 K), a total of 3805 independent
271 reflections were obtained after merging (with $-11 \leq h \leq +10$, $-14 \leq k \leq +13$ and $-7 \leq l \leq +9$, Laue
272 group -1, $R_{\text{Friedel}} = 0.0583$; Table 4 - *deposited*), out of which 3574 with $F_o > 4\sigma(F_o)$, with $d_{\text{min}} = 0.71$
273 Å. Further details pertaining to the data collection strategy are listed in Table 4 (*deposited*).

274 A second data set was collected on the four-circle diffractometer D19 with Cu(331)-
275 monochromated radiation (take-off angle $2\theta_M = 70^\circ$), providing neutrons with a wavelength of
276 $0.9449(1)$ Å. The same crystal of kurnakovite used for the room- T experiments was glued on a
277 vanadium pin and placed on a close-circuit displacer device operated at $20.0(5)$ K (Archer and Lehmann
278 1986). The measurement strategy consists of ω scans of 64 or 79° with steps of 0.07° at different χ
279 and φ positions. A total of 25 ω -scans were collected to complete almost half-Ewald sphere. Also in
280 this case: the data collection was performed using the MAD software from ILL, indexing and unit-
281 cell metrical determination was done by using PFIND and DIRAX programs, and integration of the
282 raw data and refinement of the UB-matrix were done using RETREAT and RAFD19 programs. Even
283 at low T , the lattice was found to be metrically triclinic, without any significant variation with respect
284 to the unit-cell configuration obtained at room T . A total of 10334 reflections were integrated (with
285 $-15 \leq h \leq +15$, $-5 \leq k \leq +18$ and $-11 \leq l \leq +11$, Laue group -1, $R_{\text{Friedel}} = 0.0536$, Table 4 - *deposited*),
286 out of which 5278 with $F_o > 4\sigma(F_o)$, with $d_{\text{min}} = 0.54$ Å. Further details pertaining to the data collection
287 strategy are listed in Table 4 (*deposited*).

288 Both the neutron intensity data sets (*i.e.*, collected at 293 and 20 K) were processed with the
289 program *E-STATISTICS*, implemented in the WinGX package (Farrugia 1999). The Wilson plot and
290 the statistics of distributions of the normalized structure factors (E values) suggested that the structure
291 of kurnakovite is centrosymmetric at $>75\%$ likelihood. Anisotropic crystal-structure refinements,
292 based on the intensity data collected at room and at low T , were conducted in the space group $P-1$
293 using the SHELXL-97 software (Sheldrick 1997, 2008), starting from the structure model of Corazza
294 (1974), without any H atom. The neutron scattering lengths of Mg, B, O and H were taken from Sears
295 (1986). Secondary isotropic extinction effect was corrected according to the formalism of Larson
296 (1967). For both the refinements (*i.e.*, at 293 and at 20 K), convergence was rapidly achieved after
297 the first cycles, with a series of intense negative residual peaks in the final difference-Fourier map of

298 the nuclear density, assigned to the H sites in the next cycles (*i.e.*, H has a negative neutron scattering
299 length). Shape and magnitude of the minima in the difference-Fourier maps of the nuclear density
300 showed no evidence of positional or dynamic disorder of the H sites. At the end of the refinements
301 (with $R_1(F) = 0.0693$ at 293 K, for 3574obs./291par.; $R_1(F) = 0.0415$ at 20 K, for 5278obs./275par.,
302 Table 4 - *deposited*), the variance-covariance matrix showed no significant correlation among the
303 refined variables. In addition, all variable parameters converged with all the principal mean-square
304 atomic displacement parameters positive, including those for the H sites. Further details pertaining to
305 structure refinement strategy are given in Table 4 (*deposited*). Atomic coordinates and displacement
306 parameters are listed in Tables 5 (*deposited*) and 6 (*deposited*); selected interatomic distances and
307 angles are given in Table 7.

308

309 **Discussion and Implications**

310 The multi-methodological approach aimed to describe the chemical composition of the
311 kurnakovite sample used in this study corroborates the general findings previously reported in the
312 literature: the ideal formula of this borate is $\text{MgB}_3\text{O}_3(\text{OH})_5 \cdot 5\text{H}_2\text{O}$. Mg (CN = 6) is replaced by a very
313 modest fraction of Ca and Fe^{2+} (with $\text{CaO} + \text{FeO} < 0.06$ wt%, Tables 2 and 3); the only potential
314 substituent of B (in CN = 4) is represented by Si (with $\text{SiO}_2 \approx 0.23$ wt%, Tables 2 and 3), though we
315 cannot exclude that the measured fraction of Si is the effect of mineral impurities (*e.g.*, quartz) in the
316 massive sample of kurnakovite used for the wet chemical analysis (Tables 1 and 2). The fraction of
317 other minor elements and of the REE is, overall, insignificant. The fluorine content, as potential OH-
318 group substituent, is also insignificant (*i.e.*, ~ 0.008 wt%). These experimental findings show that
319 kurnakovite does not allow any significant isomorphic substitution. The principal implications of
320 these results are:

321 1) kurnakovite cannot act as geochemical trap of industrially relevant elements (*e.g.*, Li, Be or
322 REE),

323 2) the almost ideal composition makes kurnakovite as a potentially good B-rich aggregate in
324 concretes, avoiding the risk to release undesirable elements, for example sodium, which could
325 promotes deleterious reactions for the durability of Portland or other kinds of cements.

326 In the framework of a long term project to select new potential borates as B-bearing aggregates,
327 we have reported similar findings for another mineral borate: colemanite (ideally $\text{CaB}_3\text{O}_4(\text{OH})_3 \cdot \text{H}_2\text{O}$).
328 Even for colemanite, no significant isomorphic substituents were found (Lotti et al. 2018, 2019). On
329 this basis, we are inclined to consider that the unusually high level of purity is not a peculiarity of
330 kurnakovite from the Kramer Deposit, as the colemanite that we have recently studied is from a

331 different deposit (*i.e.*, Bigadiç Mine, Balıkesir Province, Marmara Region, Turkey; Lotti et al. 2018,
332 2019), but it is rather a common feature of the hydrous borates from lacustrine deposits with
333 hydrothermal activity. We cannot exclude that, in such a geological environment, crystal nucleation
334 and growth promote purification by iterated dissolution and recrystallization. However, a higher
335 number of evidence is necessary to corroborate this potential mechanism.

336 The neutron structure model obtained in this study, based on intensity data collected at 293 and
337 20 K, is consistent with that previously reported by Corazza (1974), by single-crystal X-ray intensity
338 data (at ambient T), and the model obtained by DFT calculation (and additional ^{11}B and ^{25}Mg NMR
339 data) reported by Zhou et al. (2012). The structure of kurnakovite contains: $[\text{BO}_2(\text{OH})]$ -groups in
340 triangular coordination, $[\text{BO}_2(\text{OH})_2]$ -groups in tetrahedral coordination, and $\text{Mg}(\text{OH})_2(\text{H}_2\text{O})_4$
341 octahedra, connected in $\text{Mg}(\text{H}_2\text{O})_4\text{B}_3\text{O}_3(\text{OH})_5$ -units forming (neutral) chains parallel to $[001]$ (Fig.
342 1). Chains are mutually connected to give the tri-dimensional structure only *via* H-bonding, and
343 extra-chains “zeolitic” H_2O molecules are also involved as “bridging molecules” (Figs. 1 and 2).

344 The structure refinements at 293 and at 20 K showed that:

- 345 1) The triangular $[\text{BO}_2(\text{OH})]$ -group has an almost ideal configuration, with $\Delta(\text{B3-O})_{\text{max}} \sim 0.02$
346 Å (*i.e.*, the difference between the longest and the shortest bond distances), O-B-O angles
347 ranging between 117° and 123° , and aplanarity $< 2^\circ$ (here defined as the average angle
348 described by the plane on which the 3-oxygen sites lie and each of the three independent B-
349 O_n vectors); the tetrahedral $[\text{BO}_2(\text{OH})_2]$ -groups are only slightly distorted, but differently
350 in magnitude, with $\Delta(\text{B1-O})_{\text{max}} \sim 0.07$ Å and $\Delta(\text{B2-O})_{\text{max}} \sim 0.03$ Å; the $\text{Mg}(\text{OH})_2(\text{H}_2\text{O})_4$
351 octahedron is more distorted, with $\Delta(\text{Mg-O})_{\text{max}} \sim 0.13$ Å. As expected, the B-O distances
352 are slightly different in response to the bonding configuration of the oxygen site (*i.e.*,
353 oxygen of a hydroxyl group or as a bridging site between polyhedra).
- 354 2) All the oxygen sites in the structure of kurnakovite are involved in H-bonding, as *donors* or
355 as *acceptors* (Table 7).
- 356 3) The four independent H_2O molecules (*i.e.*, H3–O2–H4, H5–O3–H6, H8–O4–H7, H14–
357 O13–H15; Table 7) show H–O–H angles ranging between 105° and 111° , still in the range
358 of the observed H–O–H angles in solid-state materials (Chiari and Ferraris 1982; Steiner
359 1998 and references therein; Gatta et al. 2008, 2012, 2019; Lotti et al. 2018). The O–H
360 distances, corrected for “riding motion effect” (following Busing and Levy 1964) range
361 between 0.96 and 0.99 Å. All the H-bonds of the H_2O molecules show O–H...O angles \geq
362 156° (Table 7), approaching a configuration energetically favourable (*i.e.*, toward linearity,
363 Steiner 1998), and $O_{\text{donor}}\dots O_{\text{acceptor}}$ distances between 2.7 and 3.0 Å (Table 7).

- 364 4) The same general considerations pertaining to the H-bond configurations of the H₂O
365 molecules can be extended to the hydroxyl groups (*i.e.*, O1–H2, O5–H9, O6–H10, O9–H11,
366 O10–H12, O12–H13, Table 7). All the O–H distances corrected for “riding motion effect”
367 range between 0.96–0.99 Å, $O_{donor} \dots O_{acceptor}$ distances range between 2.7–3.0 Å, and O–
368 H...O >150°, excluding the O10–H12, which shows a bifurcated configuration with O6 and
369 O2 as *acceptors* (with O10...O6 ~ 3.26 Å and O10–H12...O6 ~ 157°, O10...O2 ~ 3.07 Å
370 and O10–H12...O2 ~ 121°, Table 7).
- 371 5) The refinements based on the intensity data collected at 293 and 20 K provide virtually
372 identical structure models, in terms of bond distances and angles, including the H-bonds.
373 No evidence of *T*-induced phase transition occurs. The main difference is on the magnitude
374 of the atomic displacement ellipsoids: the U_{eq} values (defined as one third of the trace of
375 the orthogonalised U_{ij} tensor, Tables 5 and 6 - *deposited*) are on the average reduced by
376 60% at 20 K, if compared to their counterparts at 293 K. Some of the atomic displacement
377 ellipsoids are significantly anisotropic at 293 K (Table 6 - *deposited*, Fig. 1), but the low-*T*
378 data confirm that no static or dynamic disorder occur into the structure of kurnakovite.

379 The experimental findings of this study provide a comprehensive view about the important role
380 played by the H-bonding network into the structure of kurnakovite, as expected for a material
381 containing ~48 wt% H₂O. The 3-dimensional structure of this material is basically due to the
382 H-bonding network, providing a clue for explaining the insignificant F vs. OH substitution shown by
383 the chemical analysis (Table 2). In such a material, we could expect that any potential structural
384 instability in response to the change of the environmental variables (*i.e.*, under chemical,
385 compressional and thermal stress conditions) would affect the H-bonding network first.

386 We have also calculated the bond valence (BV) sums of the cation and anion sites, based on the
387 structural model obtained at room *T*. Mg and B sites show no significant BV sum deviations (*i.e.*, <
388 0.04 v.u.). More significant is the deviation for some of the O and H sites, which appear being slightly
389 underbonded (*e.g.*, O6, O7, O8, O9, O12 and O13 with BV sum ranging between -0.1 and -0.2 v.u.),
390 but modelling their BV with a so complex H-bonding network is not easy. We can expect that the H-
391 bonding scheme into the structure of kurnakovite is even more complex than that reported in Table
392 7, and interactions with $O_{donor} \dots O_{acceptor}$ distances > 3.0 Å and $O_{donor}-H \dots O_{acceptor}$ angles < 120°, not
393 considered in Table 7 (298 K), could play a role, though secondary. For example, an additional weak
394 H-bond with O9 as *donor* and O1 as *acceptor* cannot be excluded, being O9...O1 = 3.366(3) Å and
395 O9-H11...O1 = 115.1(3)° (at 298 K).

396 In addition to the mineralogical conditions mentioned above, even the steric constraints in the
397 kurnakovite structure can partially concur to its chemical purity. If we consider, for example, the 3-
398 membered building unit made by 1[BO₂(OH)] + 2[BO₂(OH)₂]-groups (Figs. 1 and 2), a potential Si vs.
399 B replacement (as a low fraction of Si was observed in our sample, Tables 2 and 3) at one of the
400 tetrahedral B1 or B2 site might drastically deform the 3-membered unit and is, therefore, unlikely. We
401 can extend the same consideration to other elements that usually occur in tetrahedral coordination at
402 room conditions (*e.g.*, Be, Al, P, S, ...), coupled with the fact that cations with valence number lower
403 or higher than 3+ in any of the B-sites might respectively under- or over-bond the bridging oxygen
404 atoms (*i.e.*, O5, O6, O8, O11; Figs. 1 and 2). Even the isovalent substitution of the planar [BO₂(OH)]²⁻
405 -group with *e.g.* the [CO₃]²⁻-group would generate a significant chemical strain at the local scale;
406 however, the carbon content of kurnakovite was not measured in this study (Tables 2 and 3). The
407 octahedron could have more degrees of freedom (in terms of expansion-contraction or distortion) for
408 isovalent substitution of Mg (*e.g.*, with Ca or Fe²⁺), without relevant changes of its inter-polyhedral
409 bonding configuration, mainly governed by H-bonds (see Fig. 2). Overall, the planar or tetrahedral
410 B-substitution is unlikely, but the Mg-substitution not and, in this respect, the high chemical purity
411 of kurnakovite remains surprising if we do not consider the role played by crystallization mechanisms
412 occurring at the lacustrine deposit, described above.

413 These results represent the first step of a more extended study on the chemical (*i.e.*, by leaching
414 experiments, emulating working conditions) and physical stability (at high *P* and high/low *T*
415 conditions) of kurnakovite, aimed to provide a comprehensive description of the behaviour of this
416 potential B-rich aggregate in Portland, Sorel or other kinds of cements.

417

418 **Acknowledgements**

419 The authors thank the Institut Laue-Langevin (Grenoble, France), for the allocation of the beamtime.
420 GDG and PL acknowledge the support of the Italian Ministry of Education (MIUR) through the
421 project 'Dipartimenti di Eccellenza 2018-2022'. D. Zhang and M. Kunz, along with the Associate
422 Editor O. Tschauner, are thanked for the revision of the manuscript.

423

424

425

References

- 426
427 Archer, J. and Lehmann, M.S. (1986) A simple adjustable mount for a two-stage
428 cryorefrigerator on an Eulerian cradle. *Journal of Applied Crystallography*, 19, 456-459.
- 429 Busing, W.R. and Levy, H.A. (1964) The effect of thermal motion on the estimation of bond
430 lengths from diffraction measurements. *Acta Crystallographica*, 17, 142-146.
- 431 Carter, R.S., Palevsky, H., Myers, V.W., and Hughes, D.J. (1953) Thermal neutron absorption
432 cross sections of boron and gold. *Physical Review*, 96, 716-721.
- 433 Chiari, G. and Ferraris, G. (1982) The water molecules in crystalline hydrates studied by
434 neutron diffraction. *Acta Crystallographica*, B38, 2331–2341.
- 435 Corazza, E. (1974) The crystal structure of kurnakovite: a refinement. *Acta Crystallographica*,
436 30, 2194-2199.
- 437 DiJulio, D.D., Cooper-Jensen, C.P., Perrey, H., Fissum, K., Rofors, E., Scherzinger, J., and
438 Bentley P.M. (2017) A polyethylene-B₄C based concrete for enhanced neutron shielding at neutron
439 research facilities. *Nuclear Instruments Methods*, A859, 41-46.
- 440 Duisenberg, A.J.M. (1992) Indexing in single-crystal diffractometry with an obstinate list of
441 reflections. *Journal of Applied Crystallography*, 25, 92-96.
- 442 Farrugia, L.J. (1999) WinGX suite for small-molecule single-crystal crystallography. *Journal*
443 *of Applied Crystallography*, 32, 837-838.
- 444 Gatta, G.D., Rotiroti, N., McIntyre, G.J., Guastoni, A., and Nestola, F. (2008) New insights
445 into the crystal chemistry of epididymite and eudidymite from Malosa, Malawi: a single-crystal
446 neutron diffraction study. *American Mineralogist*, 93, 1158–1165.
- 447 Gatta, G.D., McIntyre, G.J., Swanson, G.J., and Jacobsen, S.D. (2012) Minerals in cement
448 chemistry: a single-crystal neutron diffraction and Raman spectroscopic study of thaumasite,
449 Ca₃Si(OH)₆(CO₃)(SO₄)·12H₂O. *American Mineralogist*, 197, 1060–1069.
- 450 Gatta, G.D., Lotti, P., Merlini, M., Liermann, H.-P., and Fisch, M. (2013) High-pressure
451 behavior and phase stability of Al₅BO₉, a mullite-type ceramic material. *Journal of American Ceramic*
452 *Society*, 96, 2583–2592.
- 453 Gatta, G.D., Hålenius, U., Bosi, F., Cañadillas-Delgado, L., and Fernandez-Diaz, M.T. (2019)
454 Minerals in cement chemistry: A single-crystal neutron diffraction study of ettringite,
455 Ca₆Al₂(SO₄)₃(OH)₁₂·27H₂O. *American Mineralogist*, 104, 73-78.
- 456 Glinicki, M.A., Antolik, A., and Gawlicki M. (2018) Evaluation of compatibility of neutron-
457 shielding boron aggregates with Portland cement in mortar. *Construction and Building Materials*, 164,
458 731-738.

459 Larson, A.C. (1967) Inclusion of secondary extinction in least-squares calculations. *Acta*
460 *Crystallographica*, 23, 664 – 665.

461 Lotti, P., Gatta, G.D., Comboni, D., Guastella, G., Merlini, M., Guastoni, A., and Liermann, H.P.
462 (2017) High-pressure behavior and *P*-induced phase transition of $\text{CaB}_3\text{O}_4(\text{OH})_3 \cdot \text{H}_2\text{O}$ (colemanite).
463 *Journal of American Ceramic Society*, 100, 2209–2220.

464 Lotti, P., Gatta, G.D., Demitri, N., Guastella, G., Rizzato, S., Ortenzi, M.A., Magrini, F.,
465 Comboni, D., Guastoni, A., and Fernandez-Diaz, M.T. (2018) Crystal-chemistry and temperature
466 behavior of the natural hydrous borate colemanite, a mineral commodity of boron. *Physics and*
467 *Chemistry of Minerals*, 45, 405–422.

468 Lotti, P., Comboni, D., Gigli, L., Carlucci, L., Mossini, E., Macerata, E., Mariani, M., and Gatta,
469 G.D. (2019) Thermal stability and high-temperature behavior of the natural borate colemanite: An
470 aggregate in radiation-shielding concretes. *Construction and Building Materials*, 203, 679–686.

471 Morgan, V. and Erd, R.C. (1969) Minerals of the Kramer borate district, California. California
472 Division of Mines and Geology Mineral Information Service, 22, pp. 143-153 and 165-172.

473 Noble, L.F. (1926) Borate deposits in the Kramer district, Kern County, California. U.S.
474 Geological Survey Bulletin, 785, 45-61.

475 Obert, L. and Long, A.E. (1962) Underground borate mining, Kern County, California. U.S.
476 Bureau of Mines Report of Investigation, 6110, 1-12.

477 Okuno, K., Kawai, M., and Yamada, H. (2009) Development of novel neutron shielding
478 concrete. *Nuclear Technology*, 168, 545-552.

479 Palmer M.R. and Swihart, G.H. (1996) Boron Isotope Geochemistry: An Overview. In L.M.
480 Anovitz, E.S. Grew (Eds.), *Boron: Mineralogy, Petrology, and Geochemistry*, Review in Mineralogy
481 33, Mineralogical Society of America, Chantilly, pp. 709-744.

482 Petch, H.E., Pennington, K.S., and Cuthbert, J.D. (1962) On Christ's postulated boron-oxygen
483 polyions in some hydrated borates of unknown crystal structure. *American Mineralogist*, 47, 401–404.

484 Puffer, J.H. (1975) The Kramer borate mineral assemblage. *Mineralogical Record*, 6, 84-91.

485 Rauch, H., and Waschkowski, W. (2002) Neutron Scattering Lengths. In A.J. Dianoux, G.
486 Lander (Eds.), *Neutron Data Booklet*, first ed., Institut Laue Langevin, Grenoble, pp. 1-18.

487 Razmanova, Z.P., Rumonova, I.M., Belov, N.V. (1969) Crystalline structure of kurnakovite
488 $\text{Mg}_2\text{B}_6\text{O}_{11} \cdot 15\text{H}_2\text{O} = 2\text{Mg}[\text{B}_3\text{O}_3(\text{OH})_5] \cdot 5\text{H}_2\text{O}$. *Soviet Physics "Doklady"* (English Transl.), 14, 1139–
489 1142.

490 Sears, V.F. (1986) Neutron Scattering Lengths and Cross-Sections. In K. Sköld and D.L.
491 Price, Eds., Neutron Scattering, Methods of Experimental Physics, Vol. 23A, Academic Press, New
492 York, pp. 521-550.

493 Schaller, W. (1930) Borate minerals from the Kramer district, Mohave Desert, California.
494 U.S. Geological Survey Professional Paper, 158, 137-170.

495 Sheldrick, G.M. (1997) SHELXL-97. Programs for crystal structure determination and
496 refinement. University of Göttingen, Germany.

497 Sheldrick, G.M. (2008) A short history of SHELX. *Acta Crystallographica*, A64, 112-122.

498 Siefke, J.W. (1991) The Boron open Pit Mine at the Kramer Borate Deposit. The Diversity of
499 Mineral and Energy Resources of Southern California. In M.A. McKibben, ed., Soc. Econ. Geol.
500 Guidebook Series, 12, pp 4-15.

501 Steiner, T. (1998) Opening and narrowing of the water H-O-H angle by hydrogen-bonding
502 effects: Re-inspection of neutron diffraction data. *Acta Crystallographica*, B54, 464-470.

503 Wilkinson, C., Khamis, H.W., Stansfield, R.F.D., and McIntyre, G.J. (1988) Integration of
504 single-crystal reflections using area multidetectors. *Journal of Applied Crystallography*, 21, 471-478.

505 Whistler, D.P. (1984) An Early Hemingfordian (Early Miocene) Fossil Vertebrate Fauna from
506 Boron, Western Mojave Desert, California. *Contributions in Science*, 355, Allen Press, Lawrence,
507 KS, 36 pp.

508 Zhou, B., Michaelis, V.K., Pan, Y., Yao, Y., Tait, K.T., Hyde, B.C., Wren, J.E.C., Sherriff, B.L.,
509 and Kroeker, S. (2012) Crystal structure refinements of borate dimorphs inderite and kurnakovite using
510 ^{11}B and ^{25}Mg nuclear magnetic resonance and DFT calculations. *American Mineralogist*, 97, 1858-1865.

511

512

513

514

515

516

517 Table 1. REE concentration by ICP-AES (see text for details).

518

	%m/m	ICP-AES (nm)	LOD	LOQ	
519	Ce ₂ O ₃	< LOD	413.764	0.003	0.01
	Dy ₂ O ₃	< LOD	353.170	0.0001	0.0003
	Er ₂ O ₃	< LOD	369.265	0.002	0.007
520	Eu ₂ O ₃	< LOD	381.967	0.0001	0.0003
	Gd ₂ O ₃	< LOD	342.247	0.0003	0.001
521	Ho ₂ O ₃	< LOD	345.600	0.0001	0.0003
	La ₂ O ₃	0.0003	398.852	0.0001	0.0003
522	La ₂ O ₃	> LOD	408.672	0.0002	0.0006
	Lu ₂ O ₃	< LOD	261.542	0.0002	0.0006
523	Nd ₂ O ₃	< LOD	406.109	0.0002	0.0006
	Pr ₂ O ₃	< LOD	390.844	0.0002	0.0006
524	Sm ₂ O ₃	< LOD	359.260	0.0005	0.002
	Sc ₂ O ₃	< LOD	361.383	0.0005	0.002
525	Tb ₂ O ₃	< LOD	350.917	0.0005	0.002
	Tm ₂ O ₃	< LOD	313.126	0.004	0.015
526	Yb ₂ O ₃	< LOD	328.937	0.0001	0.0003
	Y ₂ O ₃	< LOD	371.029	0.0001	0.0003
527	ThO ₂	< LOD	283.730	0.001	0.004
	UO ₂	< LOD	385.958	0.01	0.04

528 *Note:* LOD: Limit of detection (3σ); LOQ: Limit of quantification (10σ)

529

530 Table 2. Concentration of other minor elements by ICP-AES (see text for details).

531

	%m/m	ICP-AES (nm)		%m/m	ICP-AES (nm)	
532	Li ₂ O	< 0.01	670.784	NiO	< 0.01	231.604
	Na ₂ O	< 0.01	589.592	CuO	< 0.01	327.393
533	K ₂ O	< 0.01	766.490	Ag ₂ O	< 0.01	328.068
	Rb ₂ O	< 0.02	780.023	ZnO	< 0.01	206.200
534	Cs ₂ O	< 0.02	455.531	CdO	< 0.01	228.802
	BeO	< 0.01	313.107	Al ₂ O ₃	< 0.02	396.153
535	CaO	0.03	317.933	Tl ₂ O	< 0.02	190.801
	BaO	< 0.02	233.527	PbO	< 0.05	220.353
536	TiO ₂	< 0.01	334.940	P ₂ O ₅	< 0.02	213.617
	ZrO ₂	< 0.01	343.823	As ₂ O ₃	< 0.02	193.696
537	V ₂ O ₅	< 0.02	292.464	Sb ₂ O ₃	< 0.02	206.836
	Cr ₂ O ₃	< 0.01	267.716	Bi ₂ O ₃	< 0.02	223.061
538	MoO ₃	< 0.02	202.031	SiO ₂	0.23	251.611
	MnO	< 0.01	257.610	SrO	< 0.01	407.771
539	Fe ₂ O ₃	0.03	238.204	B ₂ O ₃ *	/	249.677
	CoO	< 0.01	228.616	MgO*	/	285.213

* data were not reproducible and therefore discarded

540 Table 3. Representative chemical analysis of kurnakovite from Kramer Deposit (Kern County,
 541 California), with (*left side*) and without (*right side*) the SiO₂ fraction (see text for details), and
 542 empirical formulae recalculated on the basis of 13 anions.
 543
 544
 545
 546

<i>Oxides</i>	<i>Wt%</i>	<i>e.s.d.</i>	<i>Oxides</i>	<i>Wt%</i>
B ₂ O ₃	37.3	0.3	B ₂ O ₃	37.30
MgO	14.3	0.2	MgO	14.30
SiO ₂	0.23	n.d.	CaO	0.03
CaO	0.03	n.d.	Fe ₂ O ₃	0.03
Fe ₂ O ₃	0.03	n.d.	H ₂ O	48.20
H ₂ O	48.2	0.2		
TOTAL	100.09		TOTAL	99.86
<i>Elements</i>	<i>a.p.f.u.</i>		<i>Elements</i>	<i>a.p.f.u.</i>
B ³⁺	3.00		B ³⁺	3.00
Si ⁴⁺	0.01		Mg ²⁺	0.99
Mg ²⁺	0.99		Ca ²⁺	0.00
Ca ²⁺	0.00		Fe ³⁺	0.00
Fe ³⁺	0.00		H ⁺	15.00
H ⁺	14.97			
Empirical formula:			Empirical formula:	
Mg _{0.99} (Si _{0.01} B _{3.00})Σ _{3.01} O _{3.00} (OH) ₅ ·4.98H ₂ O			Mg _{0.99} B _{3.00} O _{3.00} (OH) ₅ ·5.00H ₂ O	

562
 563
 564
 565
 566
 567
 568
 569
 570
 571
 572
 573
 574
 575
 576
 577
 578
 579
 580
 581
 582
 583
 584
 585
 586
 587
 588
 589
 590
 591
 592

593

594 Table 4 (*deposited*). Details of neutron data collection and refinements of kurnakovite.

595

596

597

598	<i>T</i> (K)	293	20
599	Crystal shape	Prism	Prism
600	Crystal volume (mm)	3 x 4 x 4	3 x 4 x 4
601	Crystal colour	White	White
602	Unit-cell parameters	<i>a</i> = 8.3547(4) Å	<i>a</i> = 8.2973(2) Å
603		<i>b</i> = 10.6198(6) Å	<i>b</i> = 10.5801(2) Å
604		<i>c</i> = 6.4513(3) Å	<i>c</i> = 6.4072(1) Å
605		α = 98.860(3) °	α = 99.023(1) °
606		β = 108.986(3) °	β = 109.047(1) °
607		γ = 105.578(3) °	γ = 105.751(1) °
608		<i>V</i> = 502.73(4) Å ³	<i>V</i> = 492.73(2) Å ³
609	Chemical formula	MgB ₃ O ₃ (OH) ₅ ·5H ₂ O	MgB ₃ O ₃ (OH) ₅ ·5H ₂ O
610	Space Group	<i>P</i> -1	<i>P</i> -1
611	<i>Z</i>	2	2
612	Radiation type	Neutron CW	Neutron CW
613	Wavelength (Å)	0.8377(1), 1.4538(1)	0.9449(1)
614	Diffraction method	D9 and D19 four-circle - ILL	D19 four-circle - ILL
615	Data-collection method	ω -scans	ω -scans
616	<i>d</i> _{min.} (Å)	0.71	0.54
617		-11 ≤ <i>h</i> ≤ +10	-15 ≤ <i>h</i> ≤ +15
618		-14 ≤ <i>k</i> ≤ +13	-5 ≤ <i>k</i> ≤ +18
619		-7 ≤ <i>l</i> ≤ +9	-11 ≤ <i>l</i> ≤ +11
620	Measured reflections	4375	10334
	Unique reflections	3805	5398
	Unique reflections with <i>F</i> _o > 4σ(<i>F</i> _o)	3574	5278
	Refined parameters	291	275
	Extinction coeff.	0.085(7)	0.079(3)
	<i>R</i> _{Friedel}	0.0583	0.0536
	<i>R</i> _σ	0.0234	0.0326
	<i>R</i> ₁ (<i>F</i>) with <i>F</i> _o > 4σ(<i>F</i> _o)	0.0693	0.0413
	<i>R</i> ₁ (<i>F</i>) for all reflections	0.0746	0.0423
	<i>wR</i> ₂ (<i>F</i> ²)	0.1837	0.1053
	GooF	1.277	1.340
	Residuals (fm/Å ³)	-2.3/+1.5	-1.5 / +2.0

Note: Statistical parameters according to the Shelxl-97 definition (Sheldrick 1997, 2008).

621 Table 5 (*deposited*). Refined fractional atomic coordinates and equivalent/isotropic displacement
622 factors (\AA^2) of kurnakovite, based on the neutron structure refinements at 293 and 20 K. U_{eq} is defined
623 as one third of the trace of the orthogonalised U_{ij} tensor. All the sites show *s.o.f.* of 100%.
624
625

Site	293 K				20 K			
	<i>x/a</i>	<i>y/b</i>	<i>z/c</i>	U_{eq}	<i>x/a</i>	<i>y/b</i>	<i>z/c</i>	U_{eq}/U_{iso}
Mg	0.6526(2)	0.2322(2)	0.8017(3)	0.0085(4)	0.65354(7)	0.23142(6)	0.80344(8)	0.00303(8)
O1	0.9218(3)	0.3218(2)	0.9200(4)	0.0199(5)	0.92448(7)	0.32097(6)	0.92248(8)	0.00595(9)
O2	0.5935(3)	0.4095(2)	0.7764(4)	0.0186(5)	0.59738(7)	0.40994(6)	0.78309(9)	0.00536(8)
O3	0.3826(2)	0.1345(2)	0.6679(3)	0.0147(4)	0.38244(7)	0.13423(6)	0.66652(9)	0.00499(8)
O4	0.6694(3)	0.0347(2)	0.8080(3)	0.0132(4)	0.66948(7)	0.03406(6)	0.80729(8)	0.00452(8)
O5	0.6503(2)	0.1920(2)	0.4730(3)	0.0108(4)	0.64976(6)	0.19129(5)	0.47493(8)	0.00362(8)
O6	0.6702(3)	0.2636(2)	0.1420(3)	0.0138(4)	0.66820(7)	0.26135(6)	0.14172(8)	0.00414(8)
O7	0.8101(2)	0.1031(2)	0.2678(3)	0.0093(4)	0.80944(6)	0.10166(5)	0.26817(8)	0.00335(8)
O8	0.9332(2)	0.3341(2)	0.5058(3)	0.0103(4)	0.93375(6)	0.33366(5)	0.50644(8)	0.00314(8)
O9	0.1493(2)	0.4411(2)	0.3550(3)	0.0129(4)	0.15314(7)	0.44373(5)	0.35973(8)	0.00405(8)
O10	0.2498(3)	0.4101(2)	0.7350(3)	0.0180(4)	0.25289(7)	0.40617(6)	0.73959(8)	0.00458(8)
O11	0.1284(2)	0.2215(2)	0.4134(3)	0.0113(4)	0.12972(6)	0.22190(5)	0.40938(8)	0.00339(8)
O12	0.0148(3)	-0.0123(2)	0.2479(4)	0.0161(4)	0.01513(7)	-0.01323(6)	0.24624(8)	0.00468(8)
O13	0.2858(3)	0.2441(2)	0.0529(4)	0.0253(5)	0.28781(7)	0.24213(6)	0.05072(9)	0.00659(9)
B1	0.7692(2)	0.2272(2)	0.3509(3)	0.0065(4)	0.76854(7)	0.22622(6)	0.35149(8)	0.00209(8)
B2	0.1114(2)	0.3527(2)	0.5014(3)	0.0070(4)	0.11340(7)	0.35307(6)	0.50293(8)	0.00214(8)
B3	0.9830(2)	0.1055(2)	0.3124(3)	0.0071(4)	0.98272(7)	0.10495(5)	0.30949(8)	0.00227(8)
H1	1.0076(5)	0.3703(4)	0.0716(7)	0.0281(8)	1.0131(2)	0.3732(1)	0.0780(2)	0.0175(2)
H2	0.9685(5)	0.3354(4)	0.8030(7)	0.0296(8)	0.9705(2)	0.3361(2)	0.8042(2)	0.0198(2)
H3	0.6606(5)	0.4706(4)	0.7125(7)	0.0304(8)	0.6617(2)	0.4692(2)	0.7118(2)	0.0192(2)
H4	0.4760(5)	0.4174(4)	0.7494(7)	0.0302(8)	0.4766(2)	0.4158(2)	0.7537(2)	0.0185(2)
H5	0.2964(5)	0.1713(4)	0.5824(6)	0.0244(7)	0.2957(2)	0.1715(2)	0.5790(2)	0.0183(2)
H6	0.3185(5)	0.0487(4)	0.6837(7)	0.0274(8)	0.3152(2)	0.0479(12)	0.6821(3)	0.0191(2)
H7	0.7687(6)	0.0222(4)	0.7683(7)	0.0312(8)	0.7697(2)	0.0220(2)	0.7685(2)	0.0193(2)
H8	0.7052(5)	0.0378(4)	0.9681(6)	0.0284(8)	0.7045(2)	0.0368(2)	0.9693(2)	0.0182(2)
H9	0.5388(5)	0.1202(4)	0.3783(6)	0.0261(7)	0.5365(2)	0.1178(1)	0.3789(2)	0.0176(2)
H10	0.5524(6)	0.2601(5)	0.1374(7)	0.0363(9)	0.5499(2)	0.2596(2)	0.1378(2)	0.0183(2)
H11	0.1202(5)	0.5216(4)	0.3993(6)	0.0260(8)	0.1221(2)	0.5246(1)	0.4043(2)	0.0159(2)
H12	0.2630(7)	0.4979(5)	0.8040(9)	0.0435(11)	0.2678(2)	0.4978(1)	0.8114(2)	0.0207(2)
H13	0.9098(5)	-0.0905(4)	0.1540(7)	0.0287(8)	0.9067(2)	-0.0927(1)	0.1511(2)	0.0170(2)
H14	0.2505(7)	0.2652(5)	0.1746(9)	0.0442(11)	0.2493(2)	0.2649(2)	0.1736(2)	0.0234(2)
H15	0.2752(7)	0.3071(5)	-0.0384(9)	0.0469(12)	0.2753(2)	0.3076(2)	-0.0398(3)	0.0210(2)

626

627 Table 6 (*deposited*). Refined displacement parameters (\AA^2) in the expression: $-2\pi^2[(ha^*)^2U_{11} + \dots +$
628 $2hka^*b^*U_{12} + \dots + 2klb^*c^*U_{23}]$, based on the neutron structure refinement of kurnakovite at 293 and
629 20 K.
630

<i>T</i> = 293 K	U_{11}	U_{22}	U_{33}	U_{23}	U_{13}	U_{12}
Mg	0.0081(7)	0.0100(7)	0.0067(7)	0.0001(6)	0.0035(5)	0.0027(5)
O1	0.0139(7)	0.0274(8)	0.0167(8)	0.0029(7)	0.0087(6)	0.0024(6)
O2	0.0194(8)	0.0161(7)	0.0225(8)	0.0057(7)	0.0097(6)	0.0070(6)
O3	0.0091(7)	0.0157(7)	0.0184(7)	0.0048(6)	0.0050(6)	0.0033(6)
O4	0.0131(7)	0.0137(7)	0.0121(7)	0.0008(6)	0.0040(6)	0.0058(5)
O5	0.0103(6)	0.0146(6)	0.0079(6)	0.0008(5)	0.0060(5)	0.0028(5)
O6	0.0164(7)	0.0195(7)	0.0090(6)	0.0048(6)	0.0063(5)	0.0091(6)
O7	0.0074(6)	0.0093(6)	0.0097(6)	0.0000(6)	0.0027(5)	0.0026(5)
O8	0.0088(7)	0.0106(7)	0.0116(7)	0.0000(6)	0.0060(5)	0.0022(5)
O9	0.0133(7)	0.0130(7)	0.0130(7)	0.0037(6)	0.0074(5)	0.0022(5)
O10	0.0144(7)	0.0224(8)	0.0140(7)	-0.0009(7)	0.0030(6)	0.0076(6)
O11	0.0083(6)	0.0099(6)	0.0146(7)	0.0000(6)	0.0044(5)	0.0034(5)
O12	0.0148(7)	0.0142(7)	0.0195(7)	-0.0007(6)	0.0069(6)	0.0077(6)
O13	0.0249(8)	0.0272(8)	0.0260(8)	0.0050(8)	0.0125(7)	0.0102(6)
B1	0.0066(7)	0.0081(7)	0.0054(6)	0.0003(6)	0.0038(5)	0.0023(5)
B2	0.0060(6)	0.0072(6)	0.0080(7)	0.0006(6)	0.0041(5)	0.0016(5)
B3	0.0063(7)	0.0069(6)	0.0068(6)	-0.0009(6)	0.0021(5)	0.0022(5)
H1	0.0245(14)	0.0313(14)	0.0290(15)	0.0076(13)	0.0117(12)	0.0086(11)
H2	0.0289(14)	0.0349(15)	0.0284(14)	0.0059(13)	0.0188(12)	0.0081(12)
H3	0.0317(15)	0.0277(14)	0.0335(15)	0.0087(13)	0.0145(12)	0.0101(12)
H4	0.0287(15)	0.0298(14)	0.0329(15)	0.0058(13)	0.0127(12)	0.0116(12)
H5	0.0223(11)	0.0246(10)	0.0259(10)	0.0054(9)	0.0077(8)	0.0100(8)
H6	0.0242(13)	0.0256(14)	0.0327(14)	0.0081(13)	0.0120(11)	0.0075(11)
H7	0.0309(12)	0.0321(11)	0.0319(11)	0.0062(9)	0.0143(9)	0.0115(8)
H8	0.0300(14)	0.0325(15)	0.0229(14)	0.0074(13)	0.0101(11)	0.0109(12)
H9	0.0238(11)	0.0286(11)	0.0254(10)	0.0047(9)	0.0128(8)	0.0051(8)
H10	0.0370(17)	0.0419(16)	0.0342(15)	0.0100(14)	0.0161(13)	0.0170(13)
H11	0.0271(14)	0.0231(14)	0.0279(14)	0.0071(13)	0.0113(12)	0.0076(11)
H12	0.0429(18)	0.0424(18)	0.0408(17)	0.0022(16)	0.0142(14)	0.0150(14)
H13	0.0291(15)	0.0237(14)	0.0315(15)	0.0035(13)	0.0112(12)	0.0088(12)
H14	0.0448(18)	0.0483(18)	0.0407(17)	0.0065(16)	0.0203(15)	0.0161(14)
H15	0.0458(18)	0.0477(18)	0.0484(18)	0.0159(16)	0.0181(15)	0.0159(14)

631
632
633
634
635
636
637
638
639
640
641

642
643
644

<i>T = 20 K</i>	U_{11}	U_{22}	U_{33}	U_{23}	U_{13}	U_{12}
Mg	0.0029(1)	0.0035(2)	0.0017(1)	-0.0001(1)	0.0006(1)	0.0004(1)
O1	0.0037(1)	0.0087(2)	0.0032(1)	0.0005(1)	0.0009(1)	-0.0001(1)
O2	0.0054(2)	0.0051(2)	0.0059(2)	0.0016(1)	0.0026(1)	0.0019(1)
O3	0.0032(1)	0.0055(2)	0.0050(1)	0.0015(1)	0.0008(1)	0.0006(1)
O4	0.0046(1)	0.0050(2)	0.0031(1)	0.0003(1)	0.0010(1)	0.0014(1)
O5	0.0028(1)	0.0050(2)	0.0018(1)	-0.0002(1)	0.0012(1)	-0.0002(1)
O6	0.0041(1)	0.0063(2)	0.0020(1)	0.0011(1)	0.0010(1)	0.0018(1)
O7	0.0026(1)	0.0033(2)	0.0028(1)	-0.0004(1)	0.0006(1)	0.0002(1)
O8	0.0024(1)	0.0032(2)	0.0025(1)	-0.0005(1)	0.0007(1)	-0.0001(1)
O9	0.0046(1)	0.0039(2)	0.0033(1)	0.0009(1)	0.0019(1)	0.0007(1)
O10	0.0039(1)	0.0053(2)	0.0023(1)	-0.0005(1)	-0.0001(1)	0.0006(1)
O11	0.0025(1)	0.0028(2)	0.0036(1)	-0.0005(1)	0.0008(1)	0.0002(1)
O12	0.0041(1)	0.0038(2)	0.0050(1)	-0.0006(1)	0.0014(1)	0.0012(1)
O13	0.0072(2)	0.0071(2)	0.0056(2)	0.0011(1)	0.0029(1)	0.0025(1)
H1	0.0142(4)	0.0199(5)	0.0112(4)	0.0001(3)	0.0011(3)	0.0019(3)
H2	0.0200(4)	0.0255(6)	0.0166(4)	0.0065(4)	0.0120(4)	0.0052(4)
H3	0.0206(5)	0.0194(5)	0.0227(5)	0.0115(4)	0.0127(4)	0.0060(4)
H4	0.0134(4)	0.0211(5)	0.0226(5)	0.0070(4)	0.0071(4)	0.0077(4)
H5	0.0151(4)	0.0189(5)	0.0205(4)	0.0079(4)	0.0034(3)	0.0081(3)
H6	0.0165(4)	0.0148(5)	0.0249(5)	0.0083(4)	0.0077(4)	0.0022(4)
H7	0.0179(4)	0.0230(5)	0.0213(4)	0.0050(4)	0.0116(4)	0.0095(4)
H8	0.0215(5)	0.0249(6)	0.0099(3)	0.0070(3)	0.0058(3)	0.0095(4)
H9	0.0124(3)	0.0183(4)	0.0143(4)	-0.0006(3)	0.0043(3)	-0.0024(3)
H10	0.0126(4)	0.0291(6)	0.0183(4)	0.0095(4)	0.0080(3)	0.0108(4)
H11	0.0207(4)	0.0126(4)	0.0180(4)	0.0046(3)	0.0093(4)	0.0086(4)
H12	0.0233(5)	0.0127(5)	0.0191(4)	-0.0044(4)	0.0038(4)	0.0056(4)
H13	0.0134(4)	0.0117(4)	0.0186(4)	-0.0012(3)	0.0030(3)	0.0000(3)
H14	0.0285(6)	0.0288(6)	0.0178(4)	0.0038(4)	0.0146(4)	0.0119(5)
H15	0.0245(5)	0.0202(5)	0.0212(5)	0.0108(4)	0.0088(4)	0.0094(4)

Note: The B1, B2 and B3 sites were modelled as isotropic at 20 K

645
646
647
648
649
650
651
652
653
654
655
656
657
658
659
660

661
662
663
664
665
666
667
668
669
670
671
672
673
674
675
676
677
678
679
680
681
682
683
684
685
686
687
688
689
690
691
692
693
694
695
696
697
698
699
700
701
702
703
704

Table 7. Relevant bond distances (Å) and angles (°) based on the neutron structure refinements.

<i>T</i> = 293 K					
Mg – O1	2.014(3)	O8 – B2 – O9	111.4(2)	O5 – H9	0.962(3)
Mg – O2	2.088(3)	O8 – B2 – O10	109.8(2)	O5 – H9*	0.9796
Mg – O3	2.027(2)	O9 – B2 – O10	110.3(1)	O5...O4	2.876(2)
Mg – O4	2.145(3)	O8 – B2 – O11	111.4(1)	H9...O4	1.916(3)
Mg – O5	2.090(2)	O9 – B2 – O11	107.6(2)	O5 – H9...O4	174.2(4)
Mg – O6	2.120(2)	O10 – B2 – O11	106.2(2)		
				O6 – H10	0.965(6)
B1 – O5	1.465(2)	O11 – B3 – O7	122.8(2)	O6 – H10*	0.9904
B1 – O6	1.502(2)	O11 – B3 – O12	117.2(2)	O6...O13	3.015(3)
B1 – O7	1.512(3)	O7 – B3 – O12	120.0(2)	H10...O13	2.064(6)
B1 – O8	1.445(2)			O6 – H10...O13	167.7(5)
		O1 – H2	0.969(5)		
B2 – O8	1.458(2)	O1 – H2*	0.9806	O9 – H11	0.976(5)
B2 – O9	1.477(2)	O1...O8	2.727(3)	O9 – H11*	0.9914
B2 – O10	1.478(3)	H2...O8	1.840(5)	O9...O8	2.759(3)
B2 – O11	1.483(3)	O1 – H2...O8	150.8(4)	H11...O8	1.783(5)
				O9 – H11...O8	176.8(4)
B3 – O7	1.370(2)	O2 – H4	0.968(5)		
B3 – O11	1.361(2)	O2 – H4*	0.9818	O10 – H12	0.930(6)
B3 – O12	1.378(3)	O2...O10	2.798(3)	O10 – H12*	0.9609
		H4...O10	1.842(5)	O10...O6	3.263(3)
O1 – Mg – O3	176.7(1)	O2 – H4...O10	168.7(5)	H12...O6	2.385(6)
O1 – Mg – O2	95.6(1)	O2 – H3	0.971(5)	O10 – H12 ...O6	157.3(5)
O3 – Mg – O2	86.3(1)	O2 – H3*	0.9838	O10 ...O2	3.070(3)
O1 – Mg – O5	88.5(1)	O2...O9	2.761(3)	H12 ...O2	2.483(5)
O3 – Mg – O5	88.7(1)	H3...O9	1.835(5)	O10 – H12...O2	121.2(4)
O2 – Mg – O5	93.1(1)	O2 – H3...O9	158.4(4)		
O1 – Mg – O6	88.9(1)	H3 – O2 – H4	111.3(3)	O12 – H13	0.967(6)
O3 – Mg – O6	93.8(1)			O12 – H13*	0.9901
O2 – Mg – O6	91.3(1)	O3 – H5	0.967(5)	O12...O13	2.859(6)
O5 – Mg – O6	175.1(1)	O3 – H5*	0.9778	H13 ...O13	1.895(5)
O1 – Mg – O4	93.2(1)	O3...O11	2.705(3)	O12 – H13...O13	174.2(4)
O3 – Mg – O4	84.9(1)	H5...O11	1.741(4)		
O2 – Mg – O4	171.2(1)	O3 – H5...O11	174.5(4)	O13 – H14	0.941(7)
O5 – Mg – O4	87.1(1)	O3 – H6	0.964(4)	O13 – H14*	0.9642
O6 – Mg – O4	88.9(1)	O3 – H6*	0.9786	O13 ...O11	3.031(4)
		O3...O7	2.776(3)	H14 ...O11	2.149(7)
O8 – B1 – O5	108.4(2)	H6...O7	1.815(4)	O13 – H14...O11	155.7(5)
O8 – B1 – O6	114.1(1)	O3 – H6...O7	174.1(4)	O13 – H15	0.961(7)
O5 – B1 – O6	108.8(2)	H5 – O3 – H6	108.9(3)	O13 – H15*	0.9869
O8 – B1 – O7	110.3(2)			O13...O10	2.899(4)
O5 – B1 – O7	108.9(1)	O4 – H8	0.970(4)	H15...O10	1.948(7)
O6 – B1 – O7	106.2(2)	O4 – H8*	0.9886	O13 – H15...O10	170.2(5)
		O4...O7	2.705(2)	H14 – O13 – H15	110.9(5)
		H8...O7	1.773(4)		
		O4 – H8...O7	159.9(4)		
		O4 – H7	0.979(6)		
		O4 – H7*	0.9988		
		O4...O12	2.842(3)		
		H7...O12	1.875(6)		
		O4 – H7...O12	169.0(5)		
		H8 – O4 – H7	105.2(4)		

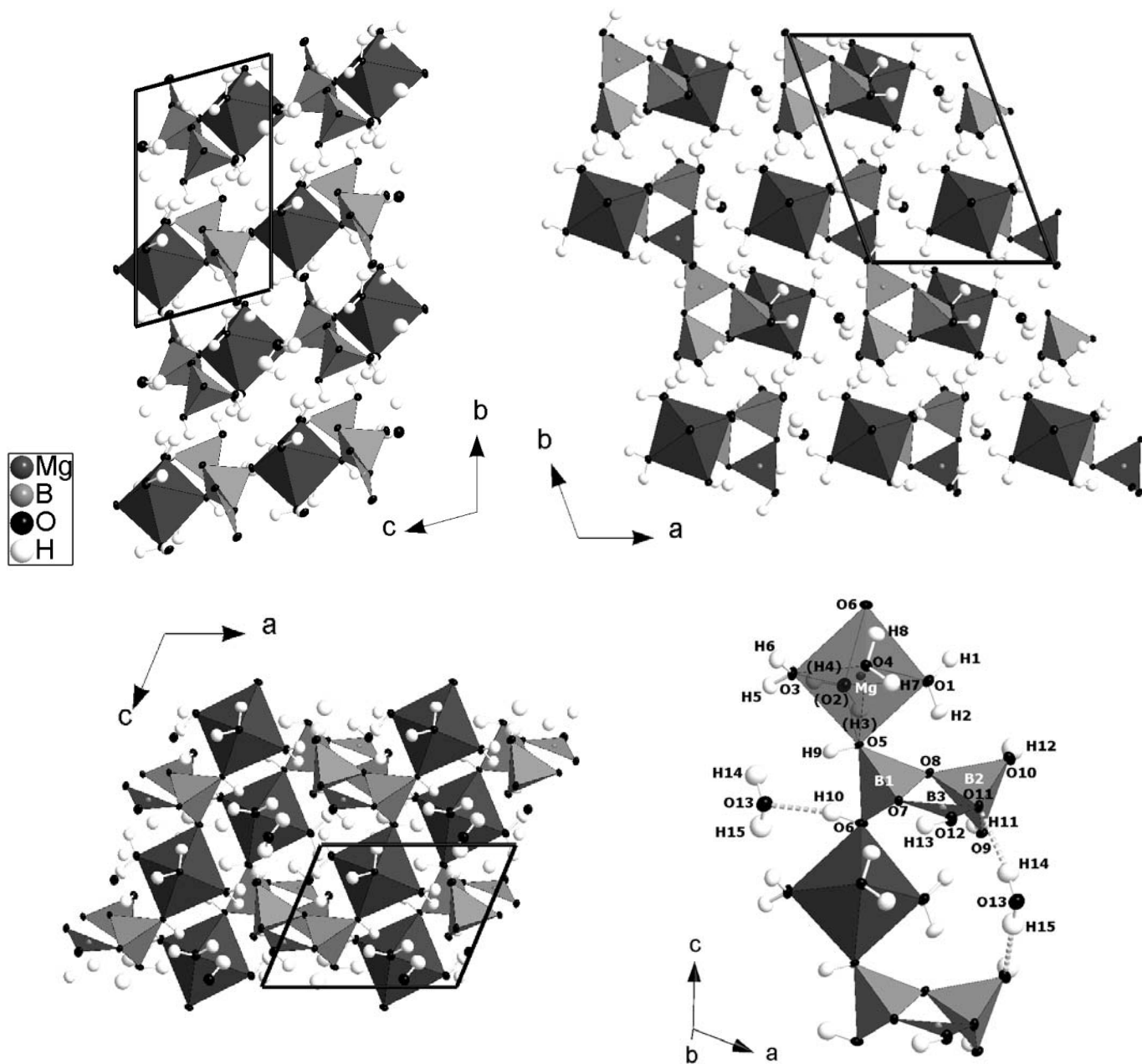
* Bond distance corrected for “riding motion” effect, following Busing and Levy (1964)

705
706
707
708
709
710
711
712
713
714
715
716
717
718
719
720
721
722
723
724
725
726
727
728
729
730
731
732
733
734
735
736
737
738
739
740
741
742
743
744
745
746
747
748
749

<i>T</i> = 20 K					
Mg – O1	2.0077(7)	O8 – B2 – O9	111.43(4)	O5 – H9	0.970(1)
Mg – O2	2.0777(8)	O8 – B2 – O10	110.05(4)	O5 – H9*	0.9887
Mg – O3	2.0150(7)	O9 – B2 – O10	111.14(4)	O5...O4	2.840(1)
Mg – O4	2.1313(8)	O8 – B2 – O11	111.50(4)	H9...O4	1.872(1)
Mg – O5	2.0690(6)	O9 – B2 – O11	107.36(4)	O5 – H9...O4	174.8(1)
Mg – O6	2.0987(6)	O10 – B2 – O11	105.18(4)		
				O6 – H10	0.969(2)
B1 – O5	1.4616(7)	O11 – B3 – O7	123.02(5)	O6 – H10*	0.9880
B1 – O6	1.4940(7)	O11 – B3 – O12	116.84(5)	O6...O13	2.959(1)
B1 – O7	1.5091(7)	O7 – B3 – O12	120.13(5)	H10...O13	2.008(1)
B1 – O8	1.4383(7)			O6 – H10...O13	166.7(1)
		O1 – H2	0.969(2)		
B2 – O8	1.4566(7)	O1 – H2*	0.9880	O9 – H11	0.985(2)
B2 – O9	1.4739(7)	O1...O8	2.715(1)	O9 – H11*	1.0003
B2 – O10	1.4794(7)	H2...O8	1.826(2)	O9...O8	2.738(1)
B2 – O11	1.4825(7)	O1 – H2...O8	151.0(1)	H11...O8	1.753(2)
				O9 – H11...O8	177.6(1)
B3 – O7	1.3638(7)	O2 – H4	0.978(2)		
B3 – O11	1.3605(7)	O2 – H4*	0.9951	O10 – H12	0.961(2)
B3 – O12	1.3766(7)	O2...O10	2.768(0)	O10 – H12*	0.9842
		H4...O10	1.803(0)	O10...O6	3.312(1)
O1 – Mg – O3	176.33(3)	O2 – H4...O10	168.5(2)	H12...O6	2.406(2)
O1 – Mg – O2	95.30(3)	O2 – H3	0.976(2)	O10 – H12 ...O6	156.9(1)
O3 – Mg – O2	86.53(3)	O2 – H3*	0.9951	O10 ...O2	3.004(1)
O1 – Mg – O5	88.56(3)	O2...O9	2.731(1)	H12 ...O2	2.381(1)
O3 – Mg – O5	88.16(3)	H3...O9	1.801(2)	O10 – H12...O2	122.0(1)
O2 – Mg – O5	93.43(3)	O2 – H3...O9	158.1(2)		
O1 – Mg – O6	89.70(3)	H3 – O2 – H4	110.9(1)	O12 – H13	0.963(2)
O3 – Mg – O6	93.45(3)			O12 – H13*	0.9859
O2 – Mg – O6	90.85(3)	O3 – H5	0.974(2)	O12...O13	2.816(3)
O5 – Mg – O6	175.52(4)	O3 – H5*	0.9913	H13 ...O13	1.840(2)
O1 – Mg – O4	93.04(3)	O3...O11	2.693(1)	O12 – H13...O13	174.2(2)
O3 – Mg – O4	85.16(3)	H5...O11	1.722(2)		
O2 – Mg – O4	171.66(3)	O3 – H5...O11	174.6(1)	O13 – H14	0.963(2)
O5 – Mg – O4	86.99(3)	O3 – H6	0.972(2)	O13 – H14*	0.9859
O6 – Mg – O4	88.98(3)	O3 – H6*	0.9903	O13 ...O11	3.003(1)
		O3...O7	2.747(1)	H14 ...O11	2.103(2)
O8 – B1 – O5	108.36(4)	H6...O7	1.777(2)	O13 – H14...O11	155.0(2)
O8 – B1 – O6	114.23(5)	O3 – H6...O7	174.9(1)	O13 – H15	0.976(2)
O5 – B1 – O6	108.85(4)	H5 – O3 – H6	108.4(1)	O13 – H15*	0.9949
O8 – B1 – O7	110.16(4)			O13...O10	2.837(1)
O5 – B1 – O7	108.91(4)	O4 – H8	0.975(1)	H15...O10	1.875(2)
O6 – B1 – O7	106.22(4)	O4 – H8*	0.9940	O13 – H15...O10	168.1(2)
		O4...O7	2.689(1)	H14 – O13 – H15	107.8(2)
		H8...O7	1.753(1)		
		O4 – H8...O7	159.6(1)		
		O4 – H7	0.975(2)		
		O4 – H7*	0.9946		
		O4...O12	2.809(1)		
		H7...O12	1.845(2)		
		O4 – H7...O12	169.2(2)		
		H8 – O4 – H7	105.4 (1)		

* Bond distance corrected for “riding motion” effect, following Busing and Levy (1964)

750 Figure 1. Three views of the crystal structure of kurnakovite along with the configuration of the
 751 $\text{Mg}(\text{H}_2\text{O})_4\text{B}_3\text{O}_3(\text{OH})_5$ -units (forming infinite chains running along $[001]$), based on the neutron
 752 structure refinement of this study (intensity data collected at 293 K). Displacement ellipsoid
 753 probability factor: 50%.
 754
 755



756
 757
 758
 759
 760
 761
 762

763
764
765
766
767
768
769
770
771
772
773
774
775
776
777
778

Figure 2. Configuration of the H-bonding network in the crystal structure of kurnakovite, based on the neutron structure refinement of this study (intensity data collected at 293 K). Displacement ellipsoid probability factor: 50%.

